CHINESE OPTICS LETTERS

Vol. 20, No. 12 | December 2022

Crystal growth and spectral properties of $(Yb_{0.15}Lu_{0.85x}Y_{0.85-0.85x})_3Al_5O_{12}$ single crystals

Ruifeng Tian (田瑞丰)[1,2], Mingyan Pan (潘明艳)[1*], Lu Zhang (张 璐)[1,2], and Hongji Qi (齐红基)[1**]

[1] Key Laboratory of Materials for High Power Laser, Shanghai Institute of Optics and Fine Mechanics, Chinese Academy of Sciences, Shanghai 201800, China

[2] University of Chinese Academy of Sciences, Beijing 100049, China

*Corresponding author: pmy@siom.ac.cn

**Corresponding author: qhj@siom.ac.cn

Received April 27, 2022 | Accepted June 23, 2022 | Posted Online August 5, 2022

Four single crystals $(Yb_{0.15}Lu_{0.85x}Y_{0.85-0.85x})_3Al_5O_{12}$ (x = 0, 0.25, 0.5, 1) were grown by the Czochralski method. The correlation of the host atom Lu:Y ratios with the density and the luminescence properties were revealed. The density increases linearly with increasing of Lu^{3+} content, which will improve the gamma ray cut-off ability. The integrated intensity of the X-ray excited luminescence spectrum increases exponentially with the increasing Y:Lu ratio, while the decay time becomes even shorter with the increasing Lu^{3+} content. These results will provide a basis to balance the comprehensive properties to match different application requirements.

Keywords: Yb:LuYAG; scintillators; Czochralski method; charge transfer.

DOI: 10.3788/COL202220.121601

1. Introduction

Inorganic scintillation crystals are widely used in high-energy particle detection, medical imaging, nuclear physics, and other fields[1]. Due to the development of high-energy physics and ultrafast pulsed radiation detection, the demand for ultrafast scintillators is becoming more and more urgent.

Ytterbium-doped yttrium aluminum garnet ($Yb:Y_3Al_5O_{12}$, Yb:YAG) is a traditional material with excellent comprehensive performance, such as good thermal conductivity, optical performance and excellent chemical stability. Up to now, Yb:YAG crystals have been widely used as high-power laser materials[2–4].

Besides, Yb:YAG is also a very important inorganic scintillator since it possesses an ultrafast decay time (0.41 ns excited by 266 nm pulsed laser)[5], which shows potential applications in pulsed radiation imaging, inertial confinement fusion (ICF) diagnosis, nuclear reaction kinetics diagnosis, and homeland security[6–9].

The study of Yb:YAG scintillators started in 1997, when Raghavan *et al.* reported that 15% (mass fraction) Yb can be used to detect low-energy solar neutrinos[10]. In 2000, van Pieterson *et al.* systematically studied the charge-transfer (CT) luminescence behavior of Yb ions in different compounds and estimated the thermal quenching temperature of Yb:YAG at $T = 80$ K[11]. In 2001, Guerassimova *et al.* reported the X-ray excited CT luminescence at $T = 80$ K. The luminescence peaks at 333 nm and 500 nm belong to CT luminescence based on the luminescence spectrum[12]. The CT state refers to the transfer process of electrons from oxygen ligands to rare earth ions (Yb^{3+}). CT luminescence refers to the energy transfer from the CT state to the two energy levels of $^2F_{7/2}$ and $^2F_{5/2}$. The Stokes shift of the CT state is 17,500 cm^{-1} reported by van Pieterson *et al.*[11], while Antonini *et al.* reported on the dependency between light yield (LY) and temperature. In more detail, the maximum LY is $(13.5 \pm 2.5) \times 10^3$ ph/MeV at 140 K for 25% Yb:YAG, and the decay time τ is shorter than 4 ns under the γ source[13].

Since Yb:YAG features extremely low LY in comparison with commercial scintillators like bismuth germanium oxide (BGO) and cesium-doped lutetium-yttrium oxyorthosilicate (Ce:LYSO), it is only suitable in the application of high-intensity pulsed gamma ray measurement. In previous studies, Chen *et al.*[7] reported that the fluence rate linear response upper limit of the Yb:YAG crystal is about 9.1×10^{18} MeV · cm^{-2} · s^{-1}, and the sensitivity of the Yb:YAG detector is 6.16×10^{20} C · cm^{-2} · MeV^{-1}. In order to further improve the detecting capacity, the gamma ray cut-off ability and the radiation hardness of the Yb:YAG single crystal should be improved.

Preliminary studies have shown that doping of host elements can modulate the crystal scintillation properties. The Ce:LuAG has better energy resolution (6.7% ± 0.3%) than Ce:YAG, while the scintillation decay time shows a longer slow component for the Ce-doped lutetium aluminum garnet (Ce:LuAG) with respect to Ce:YAG[14]. Ce:LYSO has higher LY (37,400 ± 3700 ph/MeV) but the worse energy resolution

(7.7% ± 0.2%) with respect to Ce-doped yttrium oxyorthosilicate (Ce:YSO)[15]. Thus, we can conclude that Y-Lu solid solute plays a huge role in the improvement of scintillator properties. However, Yb-doped YAG-LuAG solid solute has not been investigated systematically.

Therefore, in order to regulate the density and explore the relationship between the host atom substitution in the Yb:LuYAG system and spectral properties, we grow the single crystals of $(Yb_{0.15}Lu_{0.85x}Y_{0.85-0.85x})_3Al_5O_{12}$ ($x = 0, 0.25, 0.5, 1$) by the Czochralski method. With the same valent state and similar atom size, Lu^{3+} can substitute Y^{3+} with an arbitrary value ranging from 0 to 100% (atomic fraction). The atom fraction of Yb is 15% in all the crystals. Due to the extremely low LY of Yb:YAG crystals, the spectrally integrated intensities of the X-ray excited luminescence (XEL) spectra are widely used to evaluate their LY at room temperature. Thus, the XEL properties and decay time of the crystals were characterized and analyzed in detail.

2. Experimental Procedure

$(Yb_{0.15}Lu_{0.85x}Y_{0.85-0.85x})_3Al_5O_{12}$ ($x = 0$, 0.25, 0.5, 1) crystals were grown by the Czochralski method with a mid-frequency induction heating system. The raw materials were high-purity Yb_2O_3 (5N purity), Y_2O_3 (5N purity), Al_2O_3 (5N purity), and Lu_2O_3 (5N purity). The stoichiometry of the starting materials was weighed accurately under the formula $(Yb_{0.15}Lu_{0.85x}Y_{0.85-0.85x})_3Al_5O_{12}$ ($x = 0$, 0.25, 0.5, 1). The crystals were grown with ⟨111⟩ orientation in Ar atmosphere. The general cylindrical shape of the as-grown $(Yb_{0.15}Lu_{0.85x}Y_{0.85-0.85x})_3Al_5O_{12}$ ($x = 0.25$, 0.5, 1) is shown in Fig. 1. The crystals grow in an oxygen-deficient environment with a high concentration of oxygen vacancies. Annealing in air can reduce the defect density and remove the thermal stress during growth. All crystals were annealed at 1200°C for 12 h. The as-grown crystals were blue and changed to colorless after the annealing process. The crystals were cut and polished for optical measurements, and the size of the sample is 10 mm × 10 mm × 1 mm (Fig. 2).

The density values of the four samples were measured using the Archimedes method. The optical properties were characterized by a PerkinElmer Lambda 1050 UV/VIS/NIR spectrometer (Massachusetts, USA). The XEL spectra and decay time profiles

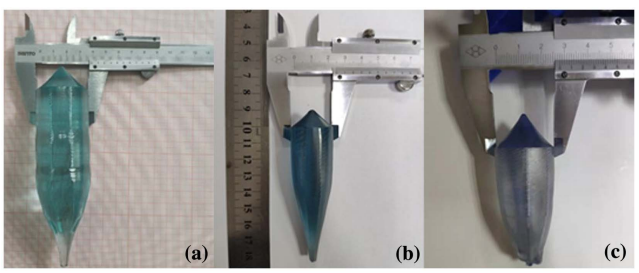

Fig. 1. Picture of the as-grown crystals for (a) $(Yb_{0.15}Lu_{0.2125}Y_{0.6375})_3Al_5O_{12}$, (b) $(Yb_{0.15}Lu_{0.425}Y_{0.425})_3Al_5O_{12}$, and (c) $(Yb_{0.15}Lu_{0.85})_3Al_5O_{12}$.

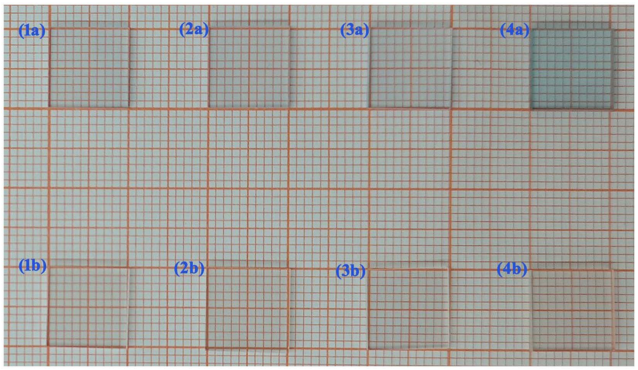

Fig. 2. Picture of the crystals for (1a), (1b) $(Yb_{0.15}Y_{0.85})_3Al_5O_{12}$, (2a), (2b) $(Yb_{0.15}Lu_{0.2125}Y_{0.6375})_3Al_5O_{12}$, (3a), (3b) $(Yb_{0.15}Lu_{0.425}Y_{0.425})_3Al_5O_{12}$, and (4a), (4b) $(Yb_{0.15}Lu_{0.85})_3Al_5O_{12}$. The samples in first and second rows are before and after annealing, respectively.

by pulse laser at 213 nm were recorded by a luminescence spectrometer (Edinburgh Instrument FLS1000, Edinburgh, UK). The X-ray source with Ag target operating at 50 kV and 15 μA was used as an excitation source. The pulse width of the pulse laser at 213 nm is 43.102 ps.

3. Results and Discussion

The density of single crystals for $(Yb_{0.15}Lu_{0.85x}Y_{0.85-0.85x})_3Al_5O_{12}$ ($x = 0$, 0.25, 0.5, 1) is shown in Table 1. The density increases linearly with increasing of Lu^{3+} content, which is consistent with Eq. (1), and the adjusted $R^2 = 0.99668$:

$$y = a + b \cdot x, \tag{1}$$

where intercept $a = 4.872$, and slope $b = 1.907$.

Transmission spectra as a function of incident wavelength (200–1200 nm) for $(Yb_{0.15}Lu_{0.85x}Y_{0.85-0.85x})_3Al_5O_{12}$ ($x = 0$, 0.25, 0.5, 1) single crystals annealed in air are shown in Fig. 3. It can be seen that the transmittance curves of these samples are similar in the range of 300–1200 nm, and the transmittance has been maintained around 80% in the range of 300–878 nm. The absorption bands of Yb^{3+} were centered at 940 nm corresponding to the 4f–4f transition. There is no significant difference in the absorption curves for the four samples

Table 1. The Densities of the Single Crystals for $(Yb_{0.15}Lu_{0.85x}Y_{0.85-0.85x})_3Al_5O_{12}$ ($x = 0$, 0.25, 0.5, 1).

Sample	Density (g/cm^3)
$(Yb_{0.15}Y_{0.85})_3Al_5O_{12}$	4.83
$(Yb_{0.15}Lu_{0.2125}Y_{0.6375})_3Al_5O_{12}$	5.40
$(Yb_{0.15}Lu_{0.425}Y_{0.425})_3Al_5O_{12}$	5.83
$(Yb_{0.15}Lu_{0.85})_3Al_5O_{12}$	6.77

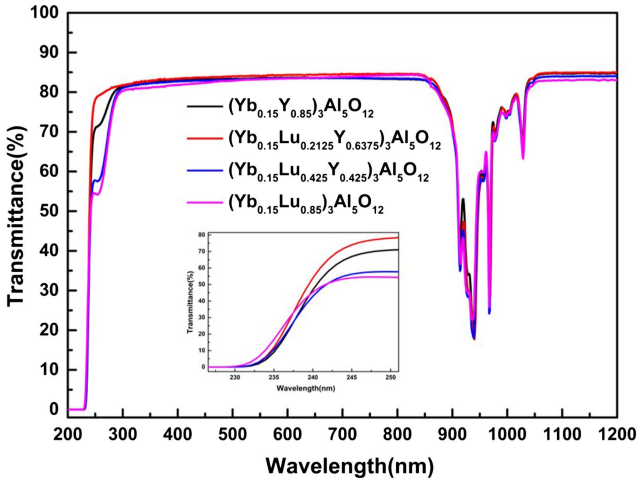

Fig. 3. Transmittance of the single crystals for $(Yb_{0.15}Lu_{0.85x}Y_{0.85-0.85x})_3Al_5O_{12}$ (x = 0, 0.25, 0.5, 1).

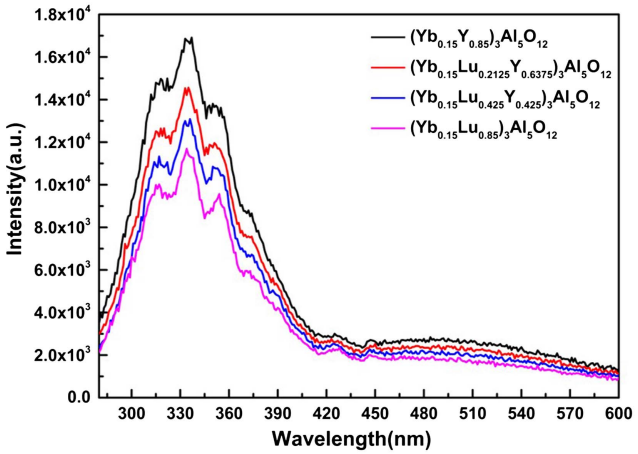

Fig. 4. XEL spectra of the single crystals for $(Yb_{0.15}Lu_{0.85x}Y_{0.85-0.85x})_3Al_5O_{12}$ (x = 0, 0.25, 0.5, 1) at room temperature.

near 940 nm. The absorption of the single crystals for $(Yb_{0.15}Lu_{0.85x}Y_{0.85-0.85x})_3Al_5O_{12}$ ($x = 0$, 0.25, 0.5, 1) below 300 nm is related to the defects and impurity in the crystals[16]. The absorption band near 255 nm, which is believed to arise from O^{2-} to Fe^{3+} CT[17]. According to the research of Fagundes-Peters *et al.*[18], Fe^{3+} impurities are usually unavoidable, which were caused by an iridium crucible and the growth environment. The Fe^{3+} ion will occupy the tetrahedral and octahedral Al^{3+} sites in the lattice[19], and a small amount of Fe^{3+} can seriously affect the induced optical losses after ultraviolet irradiation[20]. As shown in Fig. 3, $(Yb_{0.15}Lu_{0.2125}Y_{0.6375})_3Al_5O_{12}$ has the highest transmittance near 255 nm, which needs further study.

The Lu^{3+} occupies the Y^{3+} site in the $(Yb_{0.15}Lu_{0.85x}Y_{0.85-0.85x})_3Al_5O_{12}$ crystal, and the radius of the Lu^{3+} (radius = 0.083 nm) is smaller than that of the Y^{3+} (radius = 0.090 nm), resulting in a smaller ligand size around the oxygen[21,22]. Therefore, the energy of the electron transfer from the oxygen ligand to the rare earth ions increases, and the CT absorption band will appear as blue-shifted.

Figure 4 shows the XEL spectra of crystals for $(Yb_{0.15}Lu_{0.85x}Y_{0.85-0.85x})_3Al_5O_{12}$ ($x = 0$, 0.25, 0.5, 1) at room temperature. The luminescence band near 330 nm and 500 nm corresponds to the transition from the CT state to the $^2F_{7/2}$ ground state and to the $^2F_{5/2}$ excited state. The result is consistent with the report of Guerassimova *et al.*[12]. According to the position of the emission peaks in the XEL spectrum, the energy separation between $^2F_{7/2}$ and $^2F_{5/2}$ is 9761 cm^{-1} for all the samples. The energy separation is higher than 9300 cm^{-1} measured at 80 K reported by Nikl *et al.*[23], possibly due to the increase of temperature.

According to Fig. 4, the luminescence intensity of the sample gradually increases with the increase of Y^{3+} concentration, which may be related to the concentration of the defect in the crystals[24]. There is a non-stoichiometric growth phenomenon during the growth of the YAG single crystal[25]. The existence of Y_{Al} antisite defect is beneficial to the composition deviation to restore equilibrium. The antisite defects will lead to an increase in the volume of octahedral sites in the lattice[26]. Therefore, the covalency of the lattice will increase. This leads to the splitting of energy levels at the bottom of the conduction band, resulting in localized energy levels in the band gap. These localized energy levels act as carrier traps, which adversely affect the scintillation process[27]. The antisite defects concentration in the crystal is related to the radius of rare earth ions and melting point. The defects concentration increases with the decreasing rare earth ion radius[17,28]. According to Zorenko *et al.*, no antisite defects were observed in Ce:YAG single crystal films (SCFs) samples prepared at low temperatures[29]. Therefore, the antisite defect concentration may increase with increasing crystal growth temperature. The melting point of the $(Yb_{0.15}Lu_{0.85x}Y_{0.85-0.85x})_3Al_5O_{12}$ increases with the Lu^{3+} concentration[30]. Thus, the crystals with higher Lu^{3+} concentrations have higher concentrations of the antisite defects.

The relationship between Lu^{3+} concentration and XEL integral intensity in the range of 280–400 nm is shown in Fig. 5.

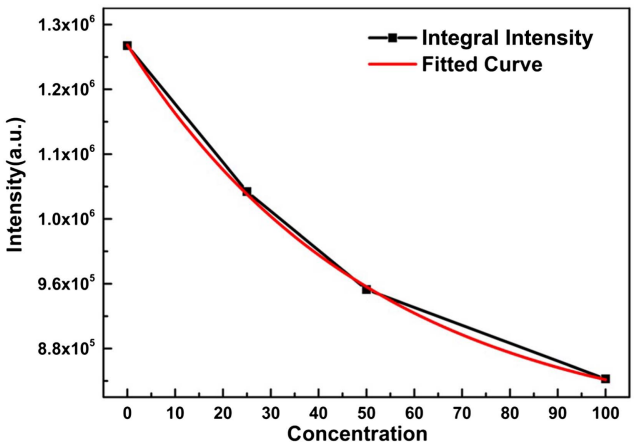

Fig. 5. Luminescence integral intensity varies with Lu^{3+} concentration increase.

The black dot plot is the integral intensity with $(Yb_{0.15}Lu_{0.85x}Y_{0.85-0.85x})_3Al_5O_{12}$, and the red curve is the fitting result. The integral intensity decreases exponentially with increasing of Lu^{3+} content in the range of 280–400 nm, which is consistent with Eq. (2), and the adjusted $R^2 = 0.99922$:

$$y = y_0 + A \cdot \exp(R_0 \cdot x). \tag{2}$$

The $(Yb_{0.15}Lu_{0.85x}Y_{0.85-0.85x})_3Al_5O_{12}$ decay time is shown in Fig. 6. All decay curves follow the single-term exponential of Eq. (3):

$$I(t) = I_0 \cdot \exp(-t/\tau), \tag{3}$$

where I_0 is the intensity at zero time, and τ is decay time.

The decay time values of the single crystals for $(Yb_{0.15}Lu_{0.85x}Y_{0.85-0.85x})_3Al_5O_{12}$ ($x = 0, 0.25, 0.5, 1$) at two wavelengths (330 nm, 500 nm) are listed in Table 2. All values were relatively close in the range of 0.78–1.34 ns, which are comparable to 0.41 ns excited by the 266 nm pulsed laser in Ref. [5]. However, Nikl *et al.*[23] reported the 340 nm luminescence decay times of Yb:YAG and Yb:LuAG at 7 K, which were 75.8 ns and 51.4 ns, respectively, much longer than the fitting results in this paper. The reason is that the luminescence decay time shortened rapidly with increasing temperature, showing an obvious temperature quenching phenomenon[31]. The decay times of each wavelength for the four samples are less than 2 ns, indicating that the $(Yb_{0.15}Lu_{0.85x}Y_{0.85-0.85x})_3Al_5O_{12}$ single crystals have a good application prospect in ultrafast scintillation.

Table 2. The Decay Time Constants of the Single Crystals for $(Yb_{0.15}Lu_{0.85x}Y_{0.85-0.85x})_3Al_5O_{12}$ ($x = 0, 0.25, 0.5, 1$) at 330 nm and 500 nm Wavelengths.

	Time Constant (ns)	
Crystal	330 nm	500 nm
$(Yb_{0.15}Y_{0.85})_3Al_5O_{12}$	1.12	1.34
$(Yb_{0.15}Lu_{0.2125}Y_{0.6375})_3Al_5O_{12}$	1.11	1.14
$(Yb_{0.15}Lu_{0.425}Y_{0.425})_3Al_5O_{12}$	1.04	1.02
$(Yb_{0.15}Lu_{0.85})_3Al_5O_{12}$	0.78	0.84

Besides, the decay times of the crystals for $(Yb_{0.15}Lu_{0.85x}Y_{0.85-0.85x})_3Al_5O_{12}$ shorten with the increasing of Lu^{3+} concentration, which shows a strong relationship. Therefore, we depict the decay time at 330 nm with the concentration of Lu^{3+} in Fig. 7 and fit the curve with Eq. (4). The curve follows a quadratic function, and the adjusted $R^2 = 0.99995$. The trend of decay time is consistent with the XEL spectrum. The variation of these decay times may be related to the change of XEL intensity. Therefore, the crystal decay time and density can be smoothly tuned by Lu^{3+} concentration:

$$y = \exp(0.11 + 6.73 \times 10^{-4} \cdot x - 4.3 \times 10^{-5} \cdot x^2). \tag{4}$$

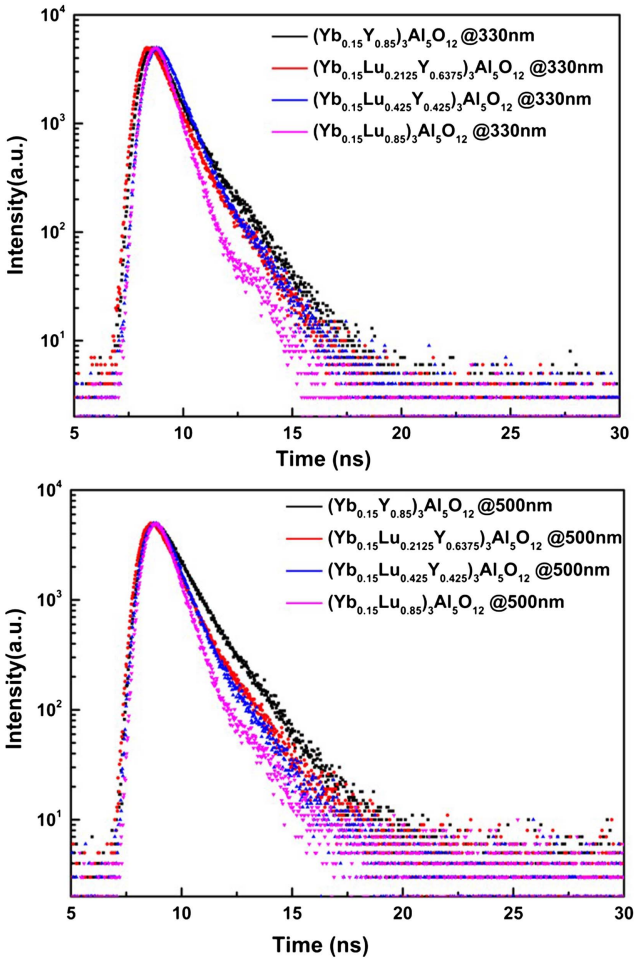

Fig. 6. 213 nm pulsed laser excited decay time profiles of the single crystals for $(Yb_{0.15}Lu_{0.85x}Y_{0.85-0.85x})_3Al_5O_{12}$ ($x = 0, 0.25, 0.5, 1$) at 330 nm and 500 nm.

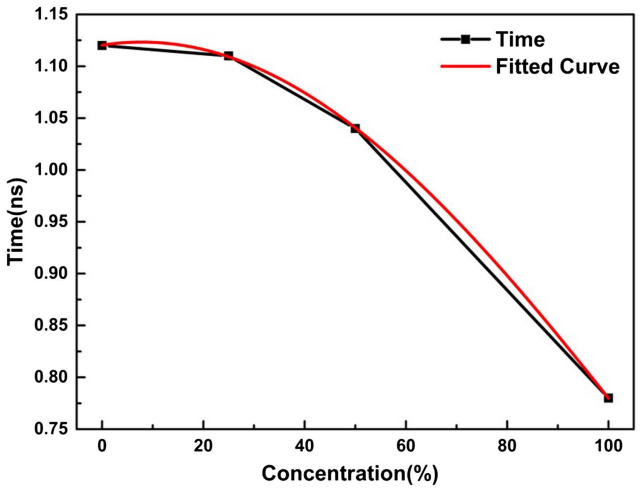

Fig. 7. Decay time of the single crystals for $(Yb_{0.15}Lu_{0.85x}Y_{0.85-0.85x})_3Al_5O_{12}$ ($x = 0, 0.25, 0.5, 1$) at 330 nm with Lu^{3+} concentration increase.

4. Conclusions

The $(Yb_{0.15}Lu_{0.85x}Y_{0.85-0.85x})_3Al_5O_{12}$ ($x = 0, 0.25, 0.5, 1$) crystals were obtained by the Czochralski method. The optical properties, XEL spectra, and luminescence decay time of the Yb-doped YAG-LuAG solid solute system were analyzed in detail. Compared with Yb:YAG, Lu^{3+} can effectively improve the effective atomic number and density of the crystal, which would have a better application prospect in the field of high-intensity detection[32]. Besides, the XEL intensity and luminescence decay time can be accurately regulated by the Lu:Y ratio, which provides flexible choices for different application scenarios.

Acknowledgement

This work was supported by the National Natural Science Foundation of China (Nos. 52002386, 52072183, and 51972319), the Shanghai Science and Technology Commission (No. 20511107400), and the Youth Innovation Promotion Association, Chinese Academy of Sciences (CAS) (No. 2021245).

References

1. M. Nikl, "Scintillation detectors for X-rays," Meas. Sci. Technol. **17**, R37 (2006).
2. M. Œwirkowicz, M. Skórczakowski, J. Jabczynski, A. Bajor, and E. Tymicki, "Investigation of structural, optical and lasing properties of YAG:Yb single crystals," Opto-Electron. Rev. **13**, 213 (2005).
3. L. Johnson, J. Geusic, and L. Van Uitert, "Coherent oscillations from Tm^{3+}, Ho^{3+}, Yb^{3+} and Er^{3+} ions in yttrium aluminum garnet," Appl. Phys. Lett. **7**, 127 (1965).
4. Y. Zhao, Q. Wang, L. Meng, Y. Yao, S. Liu, N. Cui, L. Su, L. Zheng, H. Zhang, and Y. Zhang, "Anisotropy of the thermal and laser output properties in Yb, Nd:Sc_2SiO_5 crystal," Opt. Lett. **46**, 5 (2021).
5. Z. Li, D. Tang, J. Zhang, M. Hu, and Y. Chen, "Experimental research on time response of two kinds of Yb^{3+}-doped scintillators emission spectra excited by laser," At. Energy Sci. Technol. **46**, 608 (2012).
6. K. Zhang, X. Ouyang, Z. Song, H. Han, Y. Zuo, X. Guan, X. Tan, Z. Zhang, and J. Liu, "An ideal scintillator–ZnO:Sc for sub-nanosecond pulsed radiation detection," Nucl. Instrum. **756**, 14 (2014).
7. X. Chen, Z. Zhang, K. Zhang, X. Guan, X. Weng, and H. Han, "Study on the time response of a barium fluoride scintillation detector for fast pulse radiation detection," IEEE Trans. Nucl. Sci. **67**, 1893 (2020).
8. M. Hu, Z. Li, Y. Fu, D. Tang, J. Zhang, J. Liu, R. Li, L. Chen, and Y. Huang, "The measurement of increase Yb:YAG scintillation detector pulse output electric charge," Nucl. Electron. Detect. Technol. **37**, 647 (2017).
9. K. Zhang, H. Hu, Z. Song, H. Han, X. Guan, Y. Lu, X. Chen, and Y. Yi, "Experiment investigation on pulsed gamma-ray fluence rate effect on Yb-doped yttrium aluminum garnet scintillator," Rev. Sci. Instrum. **92**, 063304 (2021).
10. R. S. Raghavan, "New prospects for real-time spectroscopy of low energy electron neutrinos from the sun," Phys. Rev. Lett. **78**, 3618 (1997).
11. L. van Pieterson, M. Heeroma, E. De Heer, and A. Meijerink, "Charge transfer luminescence of Yb^{3+}," J. Lumines. **91**, 177 (2000).
12. N. Guerassimova, N. Garnier, C. Dujardin, A. G. Petrosyan, and C. Pedrini, "X-ray excited charge transfer luminescence of ytterbium-containing aluminium garnets," Chem. Phys. Lett. **339**, 197 (2001).
13. P. Antonini, S. Belogurov, G. Bressi, G. Carugno, and P. Santilli, "Scintillation properties of Yb-doped yttrium-aluminum garnets," Nucl. Instrum. **488**, 591 (2002).
14. W. Chewpraditkul, L. Swiderski, M. Moszynski, T. Szczesniak, A. Syntfeld-Kazuch, C. Wanarak, and P. Limsuwan, "Comparative studies of $Lu_3Al_5O_{12}$:Ce and $Y_3Al_5O_{12}$:Ce scintillators for gamma-ray detection," Phys. Status Solidi A **206**, 2599 (2009).
15. C. Wanarak, A. Phunpueok, and W. Chewpraditkul, "Scintillation response of $Lu_{1.95}Y_{0.05}SiO_5$:Ce and Y_2SiO_5:Ce single crystal scintillators," Nucl. Instrum. **286**, 72 (2012).
16. S. Belogurov, G. Bressi, G. Carugno, and Y. Grishkin, "Properties of Yb-doped scintillators: YAG, YAP, LuAG," Nucl. Instrum. **516**, 58 (2004).
17. K. Mori, "Transient color-centers caused by UV light irradiation in yttrium aluminum garnet crystals," Phys. Status Solidi A **42**, 375 (1977).
18. D. Fagundes-Peters, N. Martynyuk, K. Lünstedt, V. Peters, K. Petermann, G. Huber, S. Basun, V. Laguta, and A. Hofstaetter, "High quantum efficiency YbAG-crystals," J. Lumines. **125**, 238 (2007).
19. C. Chen, G. Pogatshnik, Y. Chen, and M. R. Kokta, "Optical and electron-paramagnetic resonance studies of Fe impurities in yttrium aluminum garnet crystals," Phys. Rev. B **38**, 8555 (1988).
20. S. Rydberg and M. Engholm, "Charge transfer processes and ultraviolet induced absorption in Yb:YAG single crystal laser materials," J. Appl. Phys. **113**, 223510 (2013).
21. K. Li, S. Gan, G. Hong, and J. Zhang, "Relationship between crystal structure and luminescence properties of $(Y_{0.96-x}Ln_xCe_{0.04})_3Al_5O_{12}$ (Ln=Gd, La, Lu) phosphors," J. Rare Earths **25**, 692 (2007).
22. A. P. Anantharaman and H. P. Dasari, "Potential of pyrochlore structure materials in solid oxide fuel cell applications," Ceram. Int. **47**, 4367 (2021).
23. M. Nikl, A. Yoshikawa, and T. Fukuda, "Charge transfer luminescence in Yb^{3+}-containing compounds," Opt. Mater. **26**, 545 (2004).
24. Y. Fujimoto, M. Sugiyama, T. Yanagida, S. Wakahara, S. Suzuki, S. Kurosawa, V. Chani, and A. Yoshikawa, "Comparative study of optical and scintillation properties of Tm^{3+}:YAG, and Tm^{3+}:LuAG single crystals," Opt. Mater. **35**, 2023 (2013).
25. M. K. Ashurov, Y. K. Voronko, V. V. Osiko, A. A. Sobol, and M. I. Timoshechkin, "Spectroscopic study of stoichiometry deviation in crystals with garnet structure," Phys. Status Solidi A **42**, 101 (1977).
26. Y. Zorenko and V. Gorbenko, "Growth peculiarities of the $R_3Al_5O_{12}$ (R=Lu, Yb, Tb, Eu–Y) single crystalline film phosphors by liquid phase epitaxy," Radiat. Meas. **42**, 907 (2007).
27. M. Nikl, E. Mihokova, J. Pejchal, A. Vedda, Y. Zorenko, and K. Nejezchleb, "The antisite Lu-Al defect-related trap in $Lu_3Al_5O_{12}$: Ce single crystal," Phys. Status Solidi B **242**, R119 (2005).
28. C. R. Stanek, K. J. Mcclellan, M. R. Levy, C. Milanese, and R. W. Grimes, "The effect of intrinsic defects on $RE_3Al_5O_{12}$ garnet scintillator performance," Nucl. Instrum. **579**, 27 (2007).
29. Y. Zorenko, V. Gorbenko, I. Konstankevych, A. Voloshinovskii, G. Stryganyuk, V. Mikhallin, V. Kolobanov, and D. Spassky, "Single-crystalline films of Ce-doped YAG and LuAG phosphors: advantages over bulk crystals analogues," J. Lumines. **114**, 85 (2005).
30. Y. Kuwano, K. Suda, N. Ishizawa, and T. Yamada, "Crystal growth and properties of $(Lu, Y)_3Al_5O_{12}$," J. Cryst. Growth **260**, 159 (2004).
31. H. Ogino, A. Yoshikawa, J. H. Lee, M. Nikl, N. Solovieva, and T. Fukuda, "Growth and scintillation properties of Yb-doped $Lu_3Al_5O_{12}$ crystals," J. Cryst. Growth **253**, 314 (2003).
32. M. Nikl, A. Vedda, M. Fasoli, I. Fontana, V. V. Laguta, E. Mihokova, J. Pejchal, J. Rosa, and K. Nejezchleb, "Shallow traps and radiative recombination processes in $Lu_3Al_5O_{12}$: Ce single crystal scintillator," Phys. Rev. B **76**, 195121 (2007).